Mon. Not. R. Astron. Soc. **386,** 2015–2021 (2008) doi:10.1111/j.1365-2966.2008.13127.x

Nature versus nurture: the curved spine of the galaxy cluster X-ray luminosity–temperature relation

W. G. Hartley,[1⋆] L. Gazzola,[1] F. R. Pearce,[1] S. T. Kay[2,3] and P. A. Thomas[4]

[1]*School of Physics and Astronomy, University of Nottingham, Nottingham, NG7 2RD*
[2]*Jodrell Bank Centre for Astrophysics, School of Physics and Astronomy, The University of Manchester, Manchester M13 9PL*
[3]*Astrophysics, Department of Physics, University of Oxford, Keble Road, Oxford OX1 3RH*
[4]*Department of Physics and Astronomy, University of Sussex, Falmer, Brighton BN1 9QH*

Accepted 2008 February 19. Received 2008 January 30; in original form 2007 October 19

ABSTRACT

The physical processes that define the spine of the galaxy cluster X-ray luminosity–temperature (*L–T*) relation are investigated using a large hydrodynamical simulation of the universe. This simulation models the same volume and phases as the millennium simulation and has a linear extent of $500\,h^{-1}$ Mpc. We demonstrate that mergers typically boost a cluster along but also slightly below the *L–T* relation. Due to this boost, we expect that all of the very brightest clusters will be near the peak of a merger. Objects from near the top of the *L–T* relation tend to have assembled much of their mass earlier than an average halo of similar final mass. Conversely, objects from the bottom of the relation are often experiencing an ongoing or recent merger.

Key words: hydrodynamics – methods: numerical – cosmology: theory.

1 INTRODUCTION

Since the launch of the *XMM–Newton* and *Chandra* satellites (Jansen et al. 2001; Weisskopf et al. 2002), measurements of the X-ray emission from hot gas in clusters of galaxies have achieved unprecedented levels of accuracy and depth. However, the physical origin of the scaling relations between observable quantities, such as the luminosity of the X-ray emitting gas and its temperature, remains only partly understood.

There are currently a number of surveys (Romer, Viana & Liddle 2001; Schwope et al. 2003; Pierre et al. 2006) in progress with the potential to greatly expand our understanding of the processes that define correlations such as the luminosity–temperature (*L–T*) relation of clusters. For this potential to be realized, we require a sound theoretical basis upon which to work. To this end, numerical hydrodynamical simulations have become indispensable tools and continue to grow in size and complexity (Pearce et al. 2000; Kay, Thomas & Theuns 2003; Faltenbacher et al. 2007; Kay et al. 2007) but they have to date lacked a sufficiently large dynamic range in mass. In this work, we use a hydrodynamical model of a large volume that contains over a hundred galaxy clusters. For the first time, we are able to study the evolutionary processes within a cosmological context as we have hundreds of well-resolved objects spanning a large dynamic range rather than the more typical handful (Rowley, Thomas & Kay 2004, hereafter R04), or idealized models (Ritchie & Thomas 2002; Poole et al. 2007).

This paper is organized as follows. In the remainder of this section, we summarize the work done to date on defining the physical processes that define the shape of the *L–T* relation. Then, in Section 2, we give an account of the simulations we have undertaken, explain how our cluster subsample was selected and how the properties of these clusters were derived. Section 3 details our results before we discuss their implications and conclude in Section 4.

X-rays are chiefly emitted from the hot gas in clusters via thermal bremsstrahlung (for dark matter haloes more massive than $10^{14}\,h^{-1}\,\mathrm{M}_{\odot}$ their temperature is typically above 2 keV). For such a homologous population, Kaiser (1986) showed that simple scaling relations were expected between bulk properties such as the mass, temperature and luminosity. Observational work subsequently found that the properties of X-ray clusters were indeed related but the slopes of the relations were not those derived by Kaiser.

Kaiser (1986) assumed that galaxy clusters were self-similar entities and that therefore only a single property, such as the mass, was required in order to describe the other bulk properties. Such a homology results in an *L–T* relation with a power-law slope of two. However, as Fig. 1 demonstrates, X-ray observations of clusters with a median redshift of $\sim$0.07 found that the slope was closer to three (Markevitch 1998; Arnaud & Evrard 1999; Wu, Xue & Fang 1999; Xue & Wu 2000; Horner et al. 2001; Mulchaey et al. 2003; Osmond & Ponman 2004) and perhaps became even steeper on group scales (Helsdon & Ponman 2000).

Hydrodynamical simulations performed in the absence of cooling or any additional heat sources other than compression and shock heating have long been known to reproduce the self-similar hierarchy well (Navarro, Frenk & White 1995; Eke, Navarro & Frenk 1998). Unfortunately, they do not reproduce either the slope or the normalization of the observations, producing clusters that are too bright for any given temperature, even at the bright end. Following this work, simulations with limited physics within a cosmological

⋆E-mail: ppxwh1@nottingham.ac.uk

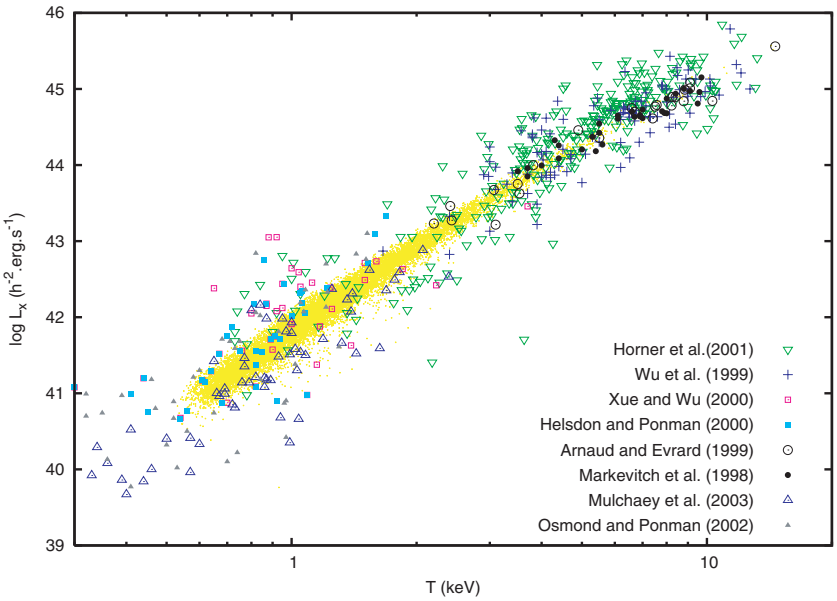

Figure 1. Compilation of low redshift observed group and cluster X-ray luminosities within r_{500} compared to their emission-weighted temperature. r_{500} is a radius enclosing an overdensity of 500. The small points are the simulated groups and clusters used in this work. The data were taken from variously: Markevitch (1998), Arnaud & Evrard (1999), Wu et al. (1999), Helsdon & Ponman (2000), Xue & Wu (2000), Horner et al. (2001), Mulchaey et al. (2003) and Osmond & Ponman (2004). Because of the pre-heating scheme, we have adopted cool cores are absent in our clusters and consequently the precise definition of temperature has a very little importance.

volume have been used in an attempt to reconcile the apparent discrepancy between theory and observation regarding the slope of the *L–T* relation (Pearce et al. 2000; Bialek, Evrard & Mohr 2001; Muanwong et al. 2001; Borgani et al. 2002, 2004). These models showed that a simple cooling or preheating scheme was sufficient to match the simulated *L–T* relation to that observed at redshift zero. More recently Kay et al. (2007) investigated the effects of feedback on the X-ray properties of clusters in hydrodynamical simulations, and demonstrated that their results were in good agreement with both the observed scaling relations and structural properties (e.g. entropy and temperature profiles), particularly for cool-core clusters.

Balogh et al. (2006) investigated the role that preheating, cooling and concentration of the halo profile can have on the scaling relations. They found that, for a realistic range of halo concentrations, the scatter generated was minimal in comparison with observed values. Variations in the cooling time of the gas in the centre of clusters could account for much of the scatter but is limited by the age of the universe and so could not explain the whole range. Finally, varying feedback from supernovae and AGN could explain the entire range, but required an order of magnitude difference in energy injection to cover the whole envelope. Their result implies that it is processed in the cores of clusters that are primarily responsible for driving the scatter in the scaling relations. This confirms earlier work by Fabian et al. (1994), Markevitch (1998) and McCarthy et al. (2004). Kay et al. (2007) identify the scatter with strong cool-core clusters, and expect the scatter to be smaller at high redshift due to the diminished prevalence of such systems. Nowadays, the general consensus is that the scatter is largely due to the strength of the X-ray core. In this work, which includes strong preheating, X-ray cores are absent. This allows us to study the shape of the relation without the additional complication of a large intrinsic scatter.

In this work, we will use a sample of haloes identified from the full simulation volume. With these we will show that because mergers tend to move clusters up the *L–T* relation they extend it beyond the point where the most massive, relaxed clusters are expected to lie. Thus, many of the brightest, most luminous objects are ongoing or recent merger events which (as R04 point out) may be difficult to resolve observationally if they are close to the peak of the merger. In addition, because we have many closely spaced outputs we can track the motion of each of our clusters on the *L–T* plane, allowing us to define a 'mean merger' vector. As this vector is not perfectly parallel to the *L–T* relation but rather falls slightly below it, a gentle roll in the relation naturally arises.

2 THE SIMULATIONS

The simulation used in this work is part of the millennium gas simulations (Pearce et al., in preparation). In this sequence of hydrodynamical simulations, all have the same volume as the millennium simulation (Springel et al. 2005) as well as utilizing the same amplitude and phase for the initial perturbations. The cosmological parameters for both the millennium simulation and the gas counterparts were: $\Omega_\Lambda = 0.75, \Omega_\mathrm{M} = 0.25, \Omega_\mathrm{b} = 0.045, h = 0.73$, $n = 1$ and $\sigma_8 = 0.9$, where the Hubble constant is characterized as $100\,h\,\mathrm{km\,s^{-1}\,Mpc^{-1}}$. These cosmological parameters are consistent with recent combined analyses from *WMAP* data (Spergel et al. 2003) and the 2dF Galaxy Redshift Survey (Colless et al. 2001). The simulation volume is a comoving cube of linear size $500\,h^{-1}\,\mathrm{Mpc}$ containing 500 million dark matter particles and 500 million gas particles. Their masses are 1.422×10^{10} and $3.12 \times 10^9\,h^{-1}\,\mathrm{M}_\odot$, respectively. The simulation includes radiative cooling of the gas, with the metalicity set at a constant value of $0.3\,\mathrm{Z}_\odot$, similar to that observed within the intracluster medium (Sarazin 1986) and preheating. The preheating is implemented in a similar way to Borgani et al. (2002): at redshift 4, the whole volume is heated to $200\,\mathrm{keV\,cm^{-2}}$ to create an entropy floor in our clusters. The value is chosen such that the resulting *L–T* relation at redshift zero matches observations. Star particles are

formed from cold, dense gas particles when a temperature threshold (2×10^4 K), a density threshold ($n_{\rm H} = 4.18 \times 10^{-27}$ g cm^{-3} and an overdensity threshold (100 times critical) are all passed, but the process of converting gas to stars has no effect on the thermal dynamics of the system, other than to make the particles collisionless. The effect of the preheating in this simulation is so extreme as to prevent any further star formation since redshift 4.

2.1 Sample selection

At redshift zero, the entire volume was processed to obtain a set of friends-of-friends haloes with a linking length of 0.2 times the mean interparticle separation. Within each of these haloes, the most bound particle was found and used as the centre for a spherical overdensity calculation that extended to r_{200}, a radius enclosing an overdensity of 200 times the cosmic mean. The analysis presented in this work is for a fixed radius of r_{500} (the radius enclosing an overdensity 500 times the cosmic mean density), roughly $0.59 \times r_{200}$ for NFW haloes (Navarro, Frenk & White 1997) of typical concentration. Within this radius, we calculate the bolometric luminosity and the emission-weighted temperature assuming a standard (Sutherland & Dopita 1993) cooling function for a uniform metalicity gas of $0.3\,{\rm Z}_{\odot}$.

Three subsamples were selected from the top, bottom and median of the *L–T* relation. We refer to the sample of clusters that are more luminous and/or cooler than expected as coming from the top of the relation, with conversely underluminous, hot clusters coming from the bottom. We also select a control sample of clusters from close to the median of the relation. The clusters were selected such that the range of masses within each sample spanned the entirety of the available relation. We only consider objects containing more than 1000 particles and that are at least two virial radii away from any larger neighbour. This ensures a meaningful estimate of the cluster bulk properties.

Once selected at redshift zero, each of our 108 clusters was traced backwards in time until their mass dropped below our imposed resolution threshold of 1000 particles. The final locations of the selected clusters on the *L–T* plane are shown on Fig. 2, where the high-scatter clusters are indicated by open circles, low scatter by open squares and the control sample by filled circles. The full sample is shown faintly in the background, together with our fitted median relation indicated by the line. Once the mass accretion histories of the sample had been extracted, a small amount of smoothing was introduced in order to remove merger-induced ringing in the cluster mass.

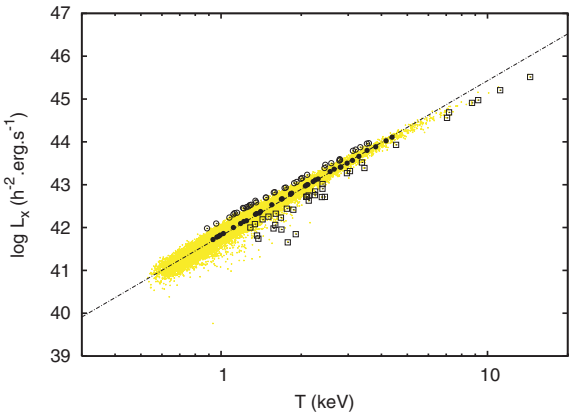

Figure 2. The clusters selected for further analysis: the high- and low-scatter samples are shown as open circles and squares, respectively, above and below the line which indicates our fitted mean relation. The control clusters are shown as solid circles. The underlying faint points show the full sample at redshift zero.

3 HALO PROPERTIES

3.1 Low-scattered haloes

The *L–T* histories of nine low-scattered haloes ranked by final mass are shown in Fig. 3, with their respective mass accretion histories given in Fig. 4. The dark track in the *L–T* plane follows the history of each object from redshift 1.5 to the present day. The background points show the location of the entire sample of clusters in the *L–T* plane at $z = 0$. To the bottom right-hand side of each panel are two additional vectors. The short line shows the mean evolution of the control sample between $z = 0.5$ and the present. The other longer line shows the evolution of each particular group over the same redshift interval. While the control sample moves slightly up in luminosity and down in temperature, eight of the nine low-scattered clusters move dramatically to larger luminosities and temperatures, nearly parallel to the spine of the *L–T* relation. This is in agreement with the trend noted by R04. Fig. 4, which shows the corresponding mass accretion histories for these objects, demonstrates that eight of the nine low-scattered objects are in the process of an ongoing major merger and are much hotter and brighter than would be typical for objects of their mass. In each of these panels, merger events are denoted by the bold sections of line. The masses at redshift 1.5 are significantly lower than expected in all bar one case (the mean mass accretion history for objects of each mass is indicated by the dotted line on Fig. 4).

3.2 High-scattered haloes

Figs 5 and 6 show the *L–T* evolution and mass accretion histories for nine of the high-scattered clusters. These nine haloes end-up significantly above the mean relation and as can be seen from their *L–T* tracks in Fig. 5, eight of the nine (all except panel e) slightly lose temperature rather than gain temperature along with the mean of the control sample. The mass accretion history makes it clear why this is the case: all bar panel (e) assemble their final mass early, with significantly more mass in place at $z = 1.5$ than that collected by the control sample. The object in panel (e) has just undergone a merger. We conclude, as did Balogh et al. (2006), that high-scattered objects are in general early forming with consequently slightly more concentrated dark matter profiles resulting in slightly more luminous objects at a particular final mass.

3.3 Properties of mergers

As discussed in the previous section, the motion of an object on the *L–T* plane during a merger is a significant driver behind finding it below the mean *L–T* relation at any given mass, particularly at the high-mass end. To explore this further, we extracted a sample of mergers from the mass accretion histories of the clusters used previously in this work. In order to distinguish a merger from gradual accretion, we require that a cluster gains significant extra mass over a short period of time. Specifically, we define a merger in the following way.

(i) A growth in mass through the merger event of at least 15 per cent of the cluster's final mass.

(ii) A ratio of at least 1:4/3 between the mass before the merger and the mass at the peak of the merger.

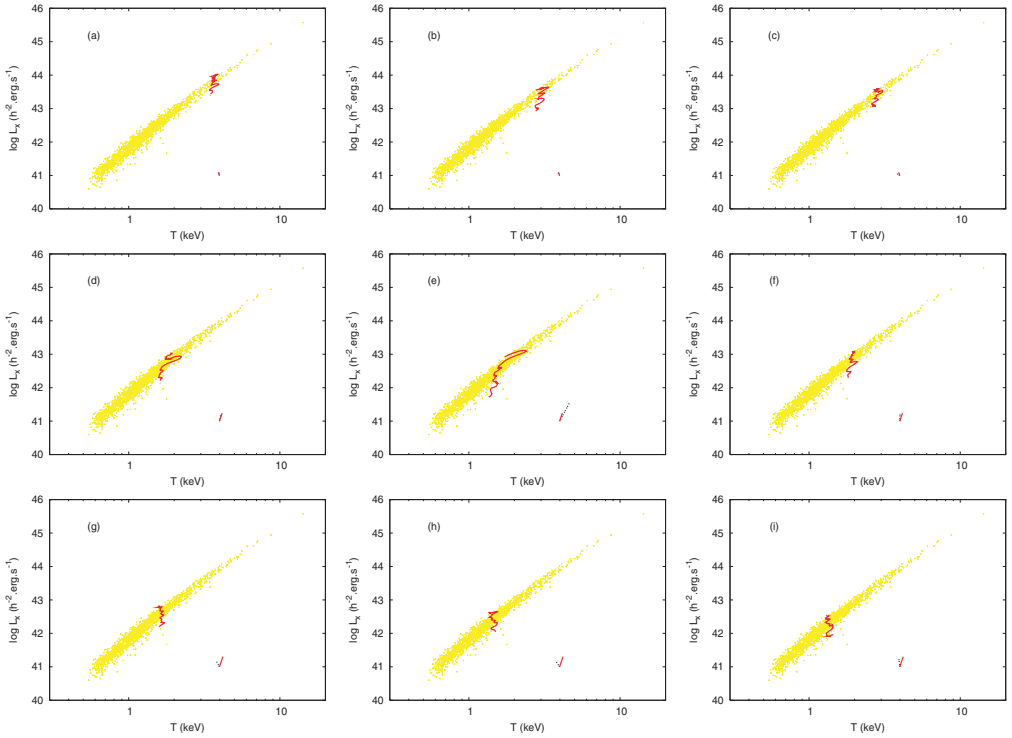

Figure 3. X-ray evolution in the *L–T* plane of nine of the low-scattered clusters ranked by final mass. In each of the nine frames, the *L–T* relation at redshift zero is defined by a sample of clusters (background points) whilst the track showing the evolution of each cluster is shown as the dark line. To the bottom right-hand side of each panel, the evolution in the *L–T* plane for each cluster (long dashed line) and the mean of the control sample members of similar mass (short solid line) between a redshift of 0.5 and zero.

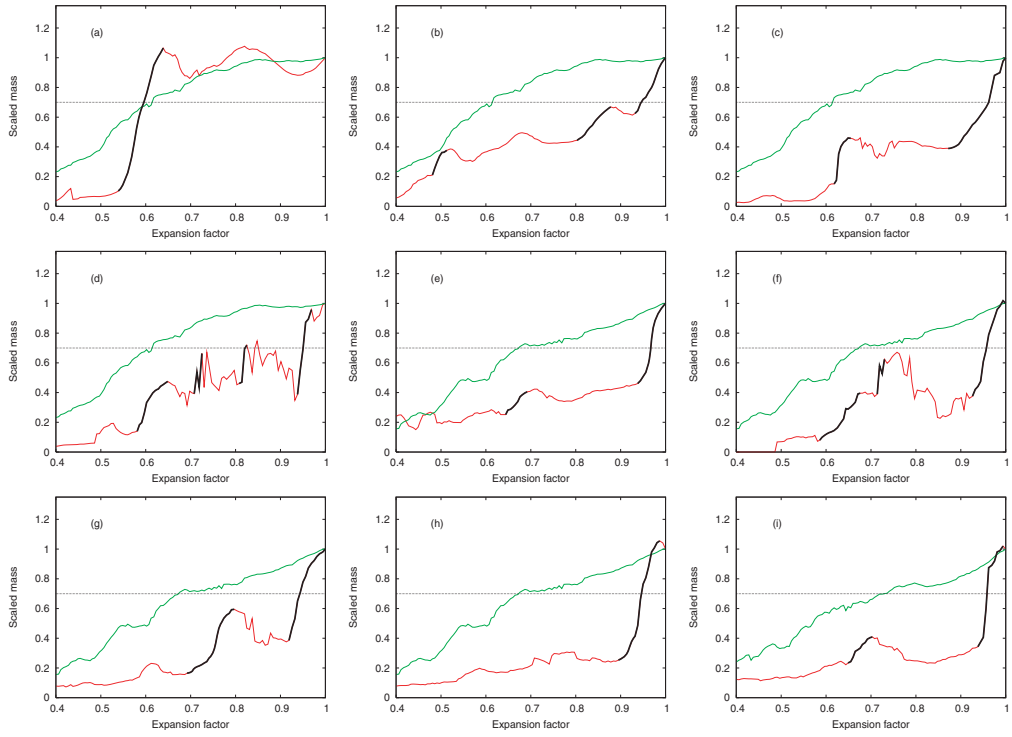

Figure 4. Mass accretion history for the nine low-scattered clusters whose *L–T* evolution was shown in Fig. 3. The lighter line is the mass accretion history for the mean of similar mass clusters in the control sample whereas the darker line shows the history of the individual cluster. Bold sections denote periods when the cluster is undergoing a merger as defined in Section 3.3 below. The mass of the cluster at each expansion factor is normalized by its final mass, labelled as 'scaled mass'. Also plotted is a horizontal dotted line to show when a cluster has assembled 70 per cent of its final mass.

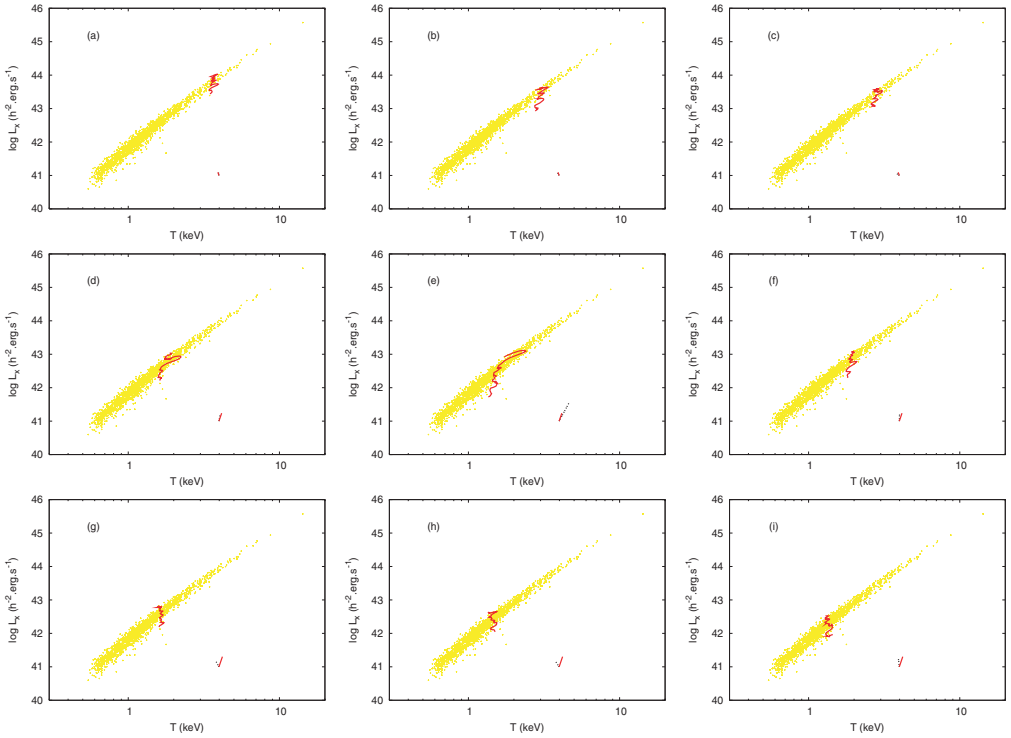

Figure 5. *L–T* evolution for nine of the high-scattered sample. The symbols and lines have the same meaning as in Fig. 3.

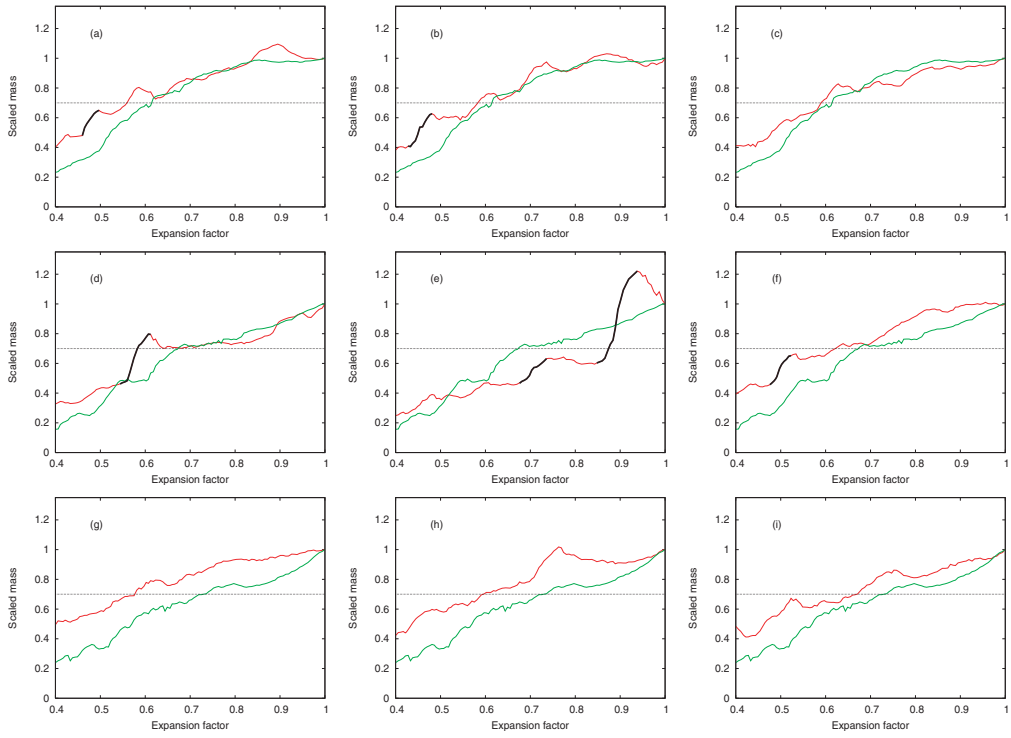

Figure 6. Mass accretion histories for the high-scattered clusters in Fig. 5. The lines have the same meanings as in Fig. 4.

(iii) The mass accretion rate must exceed 14 per cent of the final mass per Gyr.

Merger events automatically identified using this procedure are shown on the mass accretion history Figs 4 and 6 as the bold sections of the lines. The peak of a merger is considered to be the point at which the cluster's mass is greatest. As the dark matter haloes subsequently pass through each other, the final mass is usually below this value. As can immediately be guessed by simply comparing the number of bold line sections in Figs 4 and 6, the mean number of

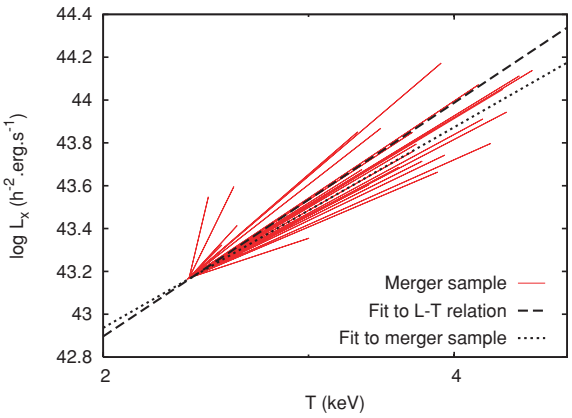

Figure 7. Relative motion on the *L–T* plane during each of the mergers defined in Section 3.3. Each line represents a single merging event. The long dashed line indicates the mean *L–T* relation whereas the dotted line indicates the mean merger direction.

mergers undergone by clusters in the low-scattered sample is over three times higher than clusters in the high-scattered sample.

By identifying the location on the *L–T* plane of each object at the start and peak of each merger we can produce a 'cricket score' diagram (Fig. 7), where each line denotes the motion on the *L–T* plane due to one merger. As the merger time-scale is short, the net drift of the relation is small while the merger is ongoing. As can be clearly seen, the net effect of a typical merger is to move an object up the relation and on average slightly below it. This tendency for mergers to fall below the mean relation is further evidenced by the large number of ongoing mergers present amongst the low-scattered objects.

Interestingly, an 'average merger' vector, indicated by the dotted line on Fig. 7, closely parallels the slope of the very high mass clusters. The tendency for mergers to boost clusters along, but at a slight angle to, the relation also drives a slight roll that is found at the high-mass end of the *L–T* relation. The slope of this vector was tested for robustness by a Jacknife Monte Carlo sampling, with the result that it is shallower than the *L–T* relation to 5σ.

4 DISCUSSION

This work examines the physics that underlies the spine of the X-ray *L–T* relation. Due to our strong preheating prescription our haloes do not have strong cores and as such do not reproduce the large scatter in the observed *L–T* relation, allowing us a clear window into the basic physics. We intend to examine the physical origin of the observed scatter in future work (Gazzola et al., in preparation) where a more physically motivated energy feedback prescription will be used and bright cooling cores are present. Preheating schemes such as the one used here are well known to accurately reproduce the slope and normalization of the *L–T* relation as a whole (Pearce et al. 2000; Bialek et al. 2001; Muanwong et al. 2001; Borgani et al. 2002). The model we have implemented also accurately reproduces the mean location of haloes on the *L–T* plane at the present day but in a much larger volume than has typically been used previously. In the real world bright cooling cores will further complicate matters but the processes discussed here which relate to the outer halo properties will underlie these, with the variation in core properties leading to a scatter about the relation discussed here.

By identifying mergers using the mass accretion histories of our objects and matching these episodes to the motion of each object on the *L–T* plane, we have derived a 'mean merger' vector in this plane. This vector lies largely parallel to the cluster *L–T* relation, as previously noted by RO4. At any particular time, the mass function of the dark matter haloes present within a volume will be exponentially truncated at the high-mass end above some characteristic mass scale. The large boost generated during a merger will produce points on the *L–T* plane appearing to lie above this characteristic mass, where there should be few objects. We therefore expect the majority of the brightest objects to be experiencing ongoing mergers, although they may be difficult to identify if they are close to their peak.

The mean merger vector we have derived is not exactly parallel to the *L–T* relation but rather lies slightly below it. This behaviour leads to all bar one of our low-scattered objects being obvious recent or ongoing merger events (Fig. 4). We also note that at the high-mass end, the vast majority of our haloes lie below the mean relation shown on Fig. 2. The fact that the mean merger vector lies slightly below the mean relation provides a natural explanation for the slight curvature evidenced in the simulated relation.

In summary, while it is straightforward to reproduce the observed slope and normalization of the X-ray *L–T* relation using a simple preheating scheme, such a scheme does not reproduce the observed scatter. As a preheating model includes the full underlying framework of the hierarchical build up of structure, bulk mergers are not significant drivers of this scatter. Mergers can, however, produce objects that are brighter and hotter than would be expected from the cluster mass as merger events drive objects along the *L–T* relation towards the bright end. We find that a typical merger track does not exactly parallel the *L–T* relation but rather lies slightly below it, leading to a prevalence of recent or ongoing merger events on the low-scattered side of the relation. This process also leads to a slight curvature of the mean relation at the high-mass end.

ACKNOWLEDGMENTS

The millennium simulation referred to in this paper was carried out by the Virgo Supercomputing Consortium at the Computing Centre of the Max-Planck Society in Garching. The millennium gas simulations were carried out at the Nottingham HPC facility, as was the analysis required by this work.

REFERENCES

Arnaud M., Evrard A. E., 1999, MNRAS, 305, 631
Balogh M. L., Babul A., Voit G. M., McCarthy I. G., Jones L. R., Lewis G. F., Ebeling H., 2006, MNRAS, 366, 624
Bialek J. J., Evrard A. E., Mohr J. J., 2001, ApJ, 555, 597
Borgani S., Governato F., Wadsley J., Menci N., Tozzi P., Quinn T., Stadel J., Lake G., 2002, MNRAS, 336, 409
Borgani S. et al., 2004, MNRAS, 348, 1078
Colless M. et al., 2001, MNRAS, 328, 1039
Eke V. R., Navarro J. F., Frenk C. S., 1998, ApJ, 503, 569
Fabian A. C., Crawford C. S., Edge A. C., Mushotzky R. F., 1994, MNRAS, 267, 779
Faltenbacher A., Hoffman Y., Gottlöber S., Yepes G., 2007, MNRAS, 145
Helsdon S. F., Ponman T. J., 2000, MNRAS, 315, 356
Horner D., Baumgartner W., Mushotzky R., Gendreau K., 2001, AAS, 1461, 33
Jansen F. et al., 2001, A&A, 365, L1
Kaiser N., 1986, MNRAS, 222, 323
Kay S. T., Thomas P. A., Theuns T., 2003, MNRAS, 343, 608
Kay S. T., da Silva A. C., Aghanim N., Blanchard A., Liddle A. R., Puget J.-L., Sadat R., Thomas P. A., 2007, MNRAS, 377, 317

McCarthy I. G., Balogh M. L., Babul A., Poole G. B., Horner D. J., 2004, ApJ, 613, 811
Markevitch M., 1998, ApJ, 504, 27
Muanwong O., Thomas P. A., Kay S. T., Pearce F. R., Couchman H. M. P., 2001, ApJ, 552, L27
Mulchaey J. S., Davis D. S., Mushotzky R. F., Burstein D., 2003, ApJS, 145, 39M
Navarro J. F., Frenk C. S., White S. D. M., 1995, MNRAS, 275, 720
Navarro J. F., Frenk C. S., White S. D. M., 1997, ApJ, 490, 493
Osmond J. P. F., Ponman T. J., 2004, MNRAS, 350, 1511
Pearce F. R., Thomas P. A., Couchman H. M. P., Edge A. C., 2000, MNRAS, 317, 1029
Pierre M. et al., 2006, MNRAS, 372, 591
Poole G. B., Babul A., McCarthy I. G., Fardal M. A., Bildfell C. G., Quinn T., Mahdavi A., 2007, MNRAS, 380, 437
Ritchie B. W., Thomas P. A., 2002, MNRAS, 329, 675
Romer A. K., Viana P. T. P., Liddle A. R., 2001, ApJ, 547, 594
Rowley D. R., Thomas P. A., Kay S. T., 2004, MNRAS, 352, 508 (R04)
Sarazin C. L., 1986, Rev. Mod. Phys., 58, 1
Schwope A. D., Lamer G., Burke D., Elvis M., Watson M. G., Schulze M. P., Szokoly G., Urrutia T., 2004, Adv. Space Res., 34, 2604
Spergel D. N. et al., 2003, ApJS, 148, 175
Springel V. et al., 2005, Nat, 435, 629
Sutherland R. S., Dopita M. A., 1993, ApJS, 88, 253
Weisskopf M. C., Brinkman B., Canizares C., Garmire G., Murray S., Van Speybroeck L. P., 2002, PASP, 114, 1
Wu X., Xue Y., Fang L., 1999, ApJ, 524, 22
Xue Y., Wu X., 2000, ApJ, 538, 65

This paper has been typeset from a TEX/LATEX file prepared by the author.